Modeling of Ignition and Combustion of High Pressure Small Orifice Diesel Sprays Using a Complex Chemical Model

J.A.J.Karlsson, T.Berglind and J.Chomiak
Department of Thermo- and Fluid Dynamics
Chalmers University of Technology
S-412, 96, Göteborg
Sweden

ABSTRACT

Detailed numerical studies of spray formation, auto-ignition, envelope flame development and combustion in a simple axi-symmetric geometry are presented for high pressure small orifice injection in order to evaluate the potential of low emission Diesel engines. An advanced spray formation model coupled with complex chemical kinetics model for n-heptane involving 17 species and 59 reactions was used in the simulation. Incorporation of the complex chemical model in a non-stationary turbulent reactive two-phase code was possible following the observation that local reaction dynamics depends on global concentration of radicals and branching agents and not on the particular nature of the species. Thus only the following 8 species are transported by the flow: reactants, sums of radicals and branching agents, intermediate fuels (CO, H_2) and products. A local stirred reactor approximation is used as a model for turbulence – chemistry interaction allowing to account for species segregation, micro-mixing and complex chemistry effects. The calculation show distinctly why high pressure, small orifice injection is superior both in NO_x and soot emissions. The main reasons are short combustion times and strong dilution of the spray by air during both premixed and diffusion combustion. The last effect, usually overlooked, is caused by very substantial flame lift-off.

INTRODUCTION

Spray combustion includes an interaction of many complex physical and chemical processes such as droplet formation, collision, coalescence, secondary break-up, evaporation, turbulence generation and modulation, as well as turbulent mixing, heat, mass and momentum transfer and chemical reactions in a highly non-uniform environment. The complex interactions make it extremely difficult to systematically study the particular effects in a well defined physical experiment, but are well suited for numerical studies based on advanced detailed models of the processes involved. The paper presents results of such a numerical experiment for high pressure small orifice injection systems which were shown experimentally to have superior emission characteristics in for instance references [1, 2, 3, 4] to name only some few important examples of the large literature of the subject. The reasons for that behavior deserve extensive investigation due to the importance of the Diesel emissions. The detailed Diesel spray combustion models known from the literature [5, 6, 7] except for the very recent one [8] use very crude chemical reaction models — either single step chemistry or eddy break-up or both with a switching criterion — and thus are unable to reproduce the very complex ignition and combustion behavior of higher hydrocarbons, particularly the negative temperature coefficients within the very important for Diesels 650 - 1000 K temperature and high pressure range. In the paper an advanced chemistry model and a new turbulence – chemistry interaction model are used to remove the limitations of current approaches. Simple axi-symmetric spray geometry is studied to reproduce the basic features of future direct injection (D.I.) Diesels with quiescent combustion systems characterized by low mechanical and heat losses and thus superior fuel economy.

THE MODEL

Spray Formation

For the spray formation and evaporation the model proposed by Reitz and Diwakar [9] and Reitz [10] was used with some modifications to improve the droplet break-up and droplet collision mechanism for high evaporation rates.

The model was adopted because it removes the need to specify the initial droplet size distribution at the nozzle which is always a serious problem.

The Chemistry

The detailed chemical kinetics of hydrocarbon combustion contains typically 1000 species and about 10 000 reactions. Reacting and transporting all these species in a

turbulent reacting code is not possible at present. A solution of this problem is to introduce generic species and a series of quasi-global reactions which represent families of individual reactions. The approach known from knock studies in homogeneous charge engines (see for instance [11] for a current review) was introduced recently into a Diesel spray model by Kong and Reitz [8]. In the application the simplest possible kinetic model was used with rate constants selected to reproduce dodecane spray ignition data in a combustion bomb. Trying to apply the model to n-heptane, the simplest fuel with a cetane number of 50, typical for contemporary Diesel fuels, for which both detailed chemistry models and fundamental ignition delay data are known we discovered however that a much more advanced chemical model is needed to reproduce the chemical behavior of the fuel over a wide range of pressure and temperatures typical for Diesel engines. To reproduce the known data [12] with a 10% accuracy and include all the basic oxidation steps of higher hydrocarbons the system shown in table 2 in appendix 1 was developed.

Chemistry – Flow Interaction

In the development of the simulation flamelet models [13] were tried with limited success. The flamelet models predicted ignition to occur at the top of the vapor jet in the rich regions a behavior not supported by experimental observations. As the whole flamelet framework seems to be questionable for Diesel auto-ignition where the ignition delay is usually many times longer than the integral time of turbulence within the spray a new turbulence – chemistry interaction model was devised based on the assumption that each computational cell is a separate stirred reactor exchanging mass and energy with neighboring cells according to the finite difference solution of the basic equations and requiring a certain turbulence time τ_m to achieve micro-mixing and allow the chemical reactions to proceed. Due to the delay in micro-mixing only a fraction of the local reactor volume is available for the chemical processes. The problem then arises how to estimate this fraction. It seems to be quite clear that it shall be proportional to the ratio of the chemical time τ_{ch} to the total conversion time in the reactor i.e. the sum of micro-mixing (eddy break-up) time τ_m and reaction time τ_{ch}. The estimate of τ_m as the ratio of turbulence kinetic energy to the energy dissipation rate $\tau_m = k/\varepsilon$ is obvious but for τ_{ch} we have so many times as reactions and thus a synthetic quantity must be selected representing the changes in the reacting system. In the global conversion the rate of energy release is the most important and thus the local reaction time may be calculated as $\tau_{ch} = \Delta h/\dot{\omega}_h$ where $\Delta h = h_b - h_u$ is the total enthalpy change during combustion and $\dot{\omega}_h$ the chemical heat release rate.

The generic reaction system still contains 17 species which are difficult to follow in a turbulent flow as 17 partial differential species equations have to be solved for that purpose. We have noticed however that the behavior of the reacting system does not depend on accurate composition of the radical and branching agent pools but only on their total concentration. Thus only the two pools have to be transported. The pools are: $[\dot{X}] = [\dot{R}] + [R\dot{O}O] + [\dot{R}OOH] + [HOOR\dot{O}O] + [HOO\dot{R}OOH] + [\dot{O}H] + [HO\dot{O}] + [\dot{H}] + 2[\dot{O}]$ and $[Y] = [ROOH] + [HOOH]$. This reduces the computational effort by almost two orders of magnitude because in addition to the reduction of the number of equations to be solved also the system stiffness is reduced very much since the rates affecting the concentration of $\dot{X}$ and Y are slow, but the rates determining the fractions of species within $\dot{X}$ and Y are very fast. We thus have the following species which are transported by the flow: Reactants (RH, O_2); Sums of radicals and branching agents ($\dot{X}$, Y); Intermediate fuels (CO, H_2); Products (CO_2, H_2O). The fractions of $\dot{R}$, $R\dot{O}O$, ..., etc. of $\dot{X}$ and $ROOH$ and $HOOH$ of Y are determined locally from the full mechanism causing that reactions quickly evolve towards the unique local system much more complex than considered in the transport equations.

COMPUTATION DETAILS

The simulation of the gas phase involves solving transient Eulerian conservation equations for mass, species, momentum, energy, turbulent kinetic energy, turbulent energy dissipation rate and the state equation. In addition to conventional single-phase flow analysis a droplet source term is added to the conservation equations representing the exchange of mass, momentum and enthalpy between the gas and the drops. For dense sprays the void fraction effect is also included in the equations. Drops effects on turbulence are not considered. Droplet motion, break-up, collisions, evaporation and turbulent diffusion are considered. The spray formation is initiated by injecting large droplets with size equal to the nozzle exit diameter with the velocity and frequency determined from the fuel flow rate, uniformly within an assumed spray angle. Open space with a side wall where the injection occurs is used as the computational domain. The initial and boundary conditions are as follows. The gas is stagnant initially. However, for numerical reasons, the kinetic energy of the turbulence of the gas and its dissipation rate are assumed to have small non-zero values. All gas properties are assumed to be uniform initially. For the gas phase a control volume formulation is used and a fully implicit "SIMPLE-C" algorithm applied except for chemical source terms. For the liquid phase Euler integration is used with explicit position, semi-implicit mass and energy and implicit momentum integration scheme. Adaptive time step is used with the limitations $\delta t < 1/2\Delta x/U_d$ and grid size (Δx) so that $\theta > 0$, where U_d is the droplet velocity and θ is the void fraction.

RESULTS AND DISCUSSION

High pressure small orifice injection is considered. For the injection pressure a 250 MPa limit is used as for this pressure some experimental data exist. Constant injection pressure is assumed for the whole injection process. Injection orifices of diameter ≥ 0.1 mm, which can be manufactured without excessive expense were studied. The combination of high pressure small orifice injection is essential because the orifice diameter to spray velocity ratio determines the local turbulence times within the spray and thus the local combustion mechanism approaching for fast mixing the distributed, homogeneous reaction with low soot and more uniform temperature i.e. low NO_x emissions. Figure 1 illustrates the auto-ignition flame formation and combustion processes for $p = 150 MPa$ and 0.1 mm orifice. Similarly as for standard injection systems ignition occurs locally in a small lean premixed region at the side of the vapor jet, moves quickly towards the stoichiometric surface as a non-adiabatic auto-ignition wave and proceeds differently in the up-steam and down-stream directions. The up-stream propagation is slow and the flame stabilizes at a certain point by a mechanism of formation of sequential ignition kernels produced in short intervals on the stoichiometric surface. The flame is wide and has a character of a distributed triple flame where the leading point is at the stoichiometric surface and the combustion occurs both on lean and rich side. The flame stabilization at a distance from the cold fuel spray allows considerable amount of air to enter the central part of the spray during the injection process. Although the spray ignition and combustion mechanism has a qualitatively universal character, considerable quantitative differences occur for high pressure – small orifice injection. The major differences are: much larger volume of the lean premixed region formed during the ignition delay, flame stabilization at a larger distance from the injection nozzle allowing much larger air entrainment in the core of the jet and it dilution. Figure 2 shows the energy release rate curves for selected cases. The maximum energy release rates are close to the ones observed experimentally for a similar case [14]. As it can be seen the ignition delay for the small orifice case does not depend on pressure. This is again in agreement with experimental data [1, 14] and follows from the negligible physical delay times. The peak energy release rates can easily be controlled by the orifice diameter and for the small diameters do not depend on injection rates. The calculation show that the rapid increase of energy release rates after ignition (Diesel knock) is due to the fast down-stream flame propagation and the following decrease to the constant values due to the up-stream flame propagation and formation of the final stationary flame. This is shown in Fig. 3 where the spray and flame development is illustrated. The figure shows the location of the maximum positive temperature gradient in the flow. Before ignition the maximum gradient occurs on the jet axis at the tip of the spray. Later on it is located at the flame edge, off-axis. One can see that the up-stream flame propagation has an oscillatory character which is due to the formation of sequential auto-ignition kernels at the edge of the flame. Thus the flame consist of an auto-ignition wave. After the flame is formed the leading point is stationary and well defined. It position defines the flame lift-off. Figure 4 shows that the flame lift-off scales well with the diameter of the orifice and is a linear function of injection velocity which indicates that the location of this point is determined by the flame stretch criterion. The flame lift-off leads to a considerable dilution of the fuel jet by air. The overall equivalence ratio of the fuel jet in the stationary diffusion burning phase is shown in Tab. 1. The strong dilution of the fuel jet by air due to the flame

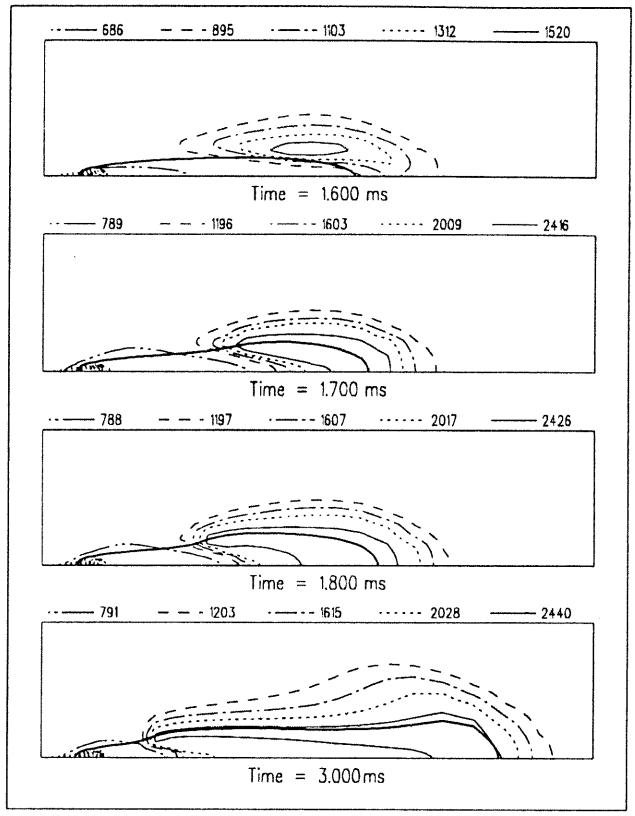

Fig. 1 Temperature field $[K]$ at different times after injection start. Constant injection speed 458 m/s during the whole calculation period. Injection nozzle diameter 0.1 mm. Air temperature 800 K, pressure 50 bar. Large chamber. Thick line shows the stoichiometric surface. Maximum spray penetration $\sim$70 mm.

Table 1 Overall equivalence ratio of the fuel jet for stationary flame.

	Pressure [MPa]		
Nozzle diameter	37	150	250
0.2 mm	3.6	—	—
0.1 mm	3.2	2.1	1.9

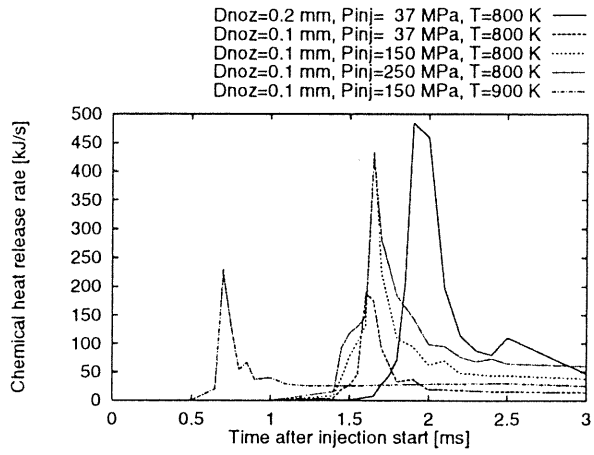

Fig. 2 Heat release rate as a function of time after injection start. Constant injection pressure and total amount of fuel (18.2 mg).

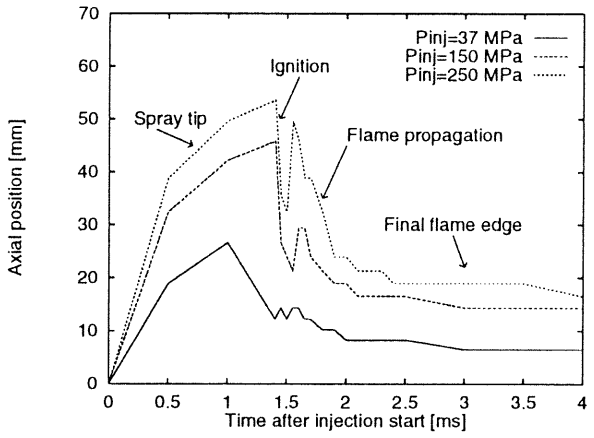

Fig. 3 Spray and flame development for nozzle diameter 0.1 *mm*.

lift-off usually overlooked in Diesel combustion analysis reduces the size of the flame, the after-burning time after injection end and the internal reaction structure leading to reduced soot and NO_x emissions for the high pressure small orifice injection cases.

CONCLUSIONS

1. Detailed numerical studies of spray formation, evaporation, ignition and combustion have been performed for high pressure small orifice injection in order to evaluate the potential of low emission Diesel engines.

2. A new turbulence – chemistry interaction model based on stirred reactor approximation accounting for species segregation, micro-mixing and non-equilibrium chemistry effects and an advanced chemical model are used in the studies.

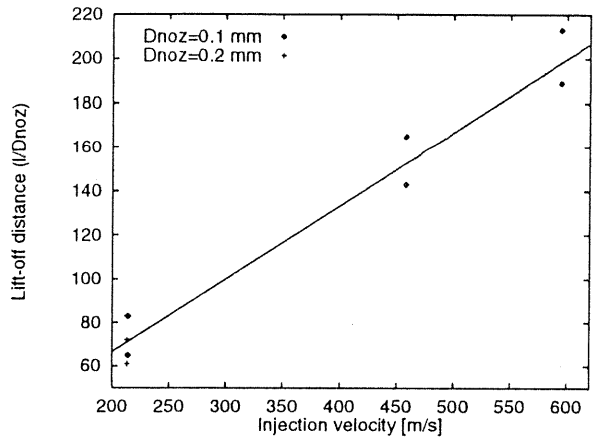

Fig. 4 Flame lift-off as a function of injection velocity.

3. The premixed flame is shown to consist of a convected non-adiabatic auto-ignition wave. The rapid down-stream propagation of the wave from the ignition point is responsible for the high initial energy release rates and Diesel knock.

4. The up-stream flame propagation has an oscillatory character and has a form of sequential ignition kernels occuring on the stoichiometric surface.

5. The final diffusion flame is stabilized at a considerable distance from the nozzle. The lift-off distance scales with flame stretch.

6. The flame lift-off leads to considerable dilution of the fuel jet by air and consequently reduces the size of the flame, the after-burning time and the internal structure leading to reduced soot and NO_x emissions for the high pressure small orifice sprays.

ACKNOWLEDGMENTS

This work was supported by grant from Volvo Research Foundation, Volvo Educational Foundation and the Swedish Board of Technological Development NUTEK.

REFERENCES

[1] Kamimoto, T., Yokota, H., and Kobayashi, H., "Effects of High Pressure Injection on Soot Formation Processes in a Rapid Compression Machine to Simulate Diesel Flames," SAE Trans. Vol. 96 Sect. 4, Paper No. 871610, pp. 783-791, 1988.

[2] Kato, T., Tsujimura, K., Shintani, M., and Minami, T., "Spray Characteristics and Combustion Improvement of D.I. Diesel Engine with High Pressure Fuel Injection," SAE Paper 890265, 1989.

[3] Zelenka, P., Kriegler, W., Herzog, P. L., and Cartellieri, W. P., "Ways Toward the Clean Heavy Duty Diesel," SAE Trans. Vol. 99 Sect. 3, Paper No. 900602, pp. 1279-1291, 1991.

[4] Herzog, P. L., Burgler, L., Winklhofer, E., Zelenka, P., and Cartellieri, W., "NO_x Reduction Strategies for D.I. Diesel Engines," SAE Trans. Vol. 101 Sect. 3, Paper No. 920470, pp. 820-836, 1993.

[5] Amsden, A. A., O'Rourke, P. J., and Butler, T. D., "KIVA-II: A Computer Program for Chemically Reactive Flows with Sprays," Los Alamos National Laboratory Report LA-11560-MS, 1989.

[6] Takagi, T., Fang, Ch. Y., Kamimoto, T., and Okamoto, T., "Numerical Simulation of Evaporation, Ignition and Combustion of Transient Sprays," Combustion Sci. and Tech. Vol. 75, pp. 1-12, 1991.

[7] Manuel, A., Gonzalez, D., Lian, Zhi. W., and Reitz, R. D., "Modeling Diesel Engine Spray Vaporization and Combustion," SAE Trans. Vol. 101 Sect. 3, Paper No. 920579, pp. 1064-1076, 1993.

[8] Kong, S. C., and Reitz, R. D., "Multidimensional Modeling of Diesel Ignition and Combustion Using a Multistep Kinetics Model," Transaction of the ASME, Journal of Engineering for Gas Turbines and Power Vol. 115, pp. 781-789, 1993.

[9] Reitz, R. D., and Diwakar, R., "Structure of High-Pressure Fuel Sprays," SAE Trans. Vol. 97 Sect. 5, Paper No. 870598, pp. 492-509, 1988.

[10] Reitz, R. D., "Modeling Atomization Processes in High Pressure Vaporizing Sprays," Atomization and Spray Technology Vol. 3, pp. 309-337, 1987.

[11] Chun, K. M., Heywood, J. B., and Keck, J. C., "Prediction of Knock Occurrence in Spark-Ignition Engine," Twenty-Second Symposium (International) on Combustion, The Combustion Institute, Pittsburgh, pp. 455-463, 1989.

[12] Ciezki, H. K., and Adomeit, G., "Shock Tube Investigation of Self-Ignition of n-Heptane – Air Mixtures Under Engine Relevant Conditions," Combustion and Flame Vol. 93, pp. 421-433, 1993.

[13] Bruel, P., Rogg, B., and Bray, K. N. C., "On Auto-Ignition in Laminar and Turbulent Non-Premixed Systems," Twenty-Third Symposium (International) on Combustion, The Combustion Institute, Pittsburgh, pp. 759-766, 1990.

[14] Yokota, H., Kamimoto, T., Kosaka, H., and Tsujimura, K., "Fast Burning and Reduced Soot Formation via Ultra-High Pressure Diesel Fuel Injection," SAE Paper 910225, 1991.

APPENDIX 1

Table 2: Rate coefficients for the generic reaction mechanism, A $[mol/m^3]$, β and E_a $[kJ]$ are the Arrhenius coefficients in $k = A\,T^{\beta}\exp(-E_a/RT)$ and $[RH]$ is evaluated as $[H_2C_{7/8}]$.

			A	β	E_a
1	$RH + O_2$	$\rightarrow \dot{R} + H\dot{O}O$	$1.11\ 10^{7}$	0.04	201.19
2	$RH + \dot{O}H$	$\rightarrow \dot{R} + H_2O$	$1.01\ 10^{3}$	1.25	3.42
3	$\dot{R} + O_2$	$\rightarrow R\dot{O}O$	$2.00\ 10^{6}$	0.00	0.00
4	$R\dot{O}O$	$\rightarrow \dot{R} + O_2$	$2.00\ 10^{15}$	0.00	117.23
5	$R\dot{O}O$	$\rightarrow \dot{R}OOH$	$5.44\ 10^{9}$	0.59	44.97
6	$\dot{R}OOH$	$\rightarrow R\dot{O}O$	$6.01\ 10^{10}$	0.59	44.97
7	$\dot{R}OOH + O_2$	$\rightarrow HOOR\dot{O}O$	$2.00\ 10^{6}$	0.00	0.00
8	$HOOR\dot{O}O$	$\rightarrow \dot{R}OOH + O_2$	$2.00\ 10^{15}$	0.00	117.23
9	$HOOR\dot{O}O$	$\rightarrow HO\dot{O}ROOH$	$1.92\ 10^{9}$	0.71	44.48
10	$HO\dot{O}ROOH$	$\rightarrow \frac{1}{16}O_2 - RH + \frac{7}{8}CO + \dot{O}H + ROOH$	$1.00\ 10^{9}$	0.00	31.40
11	$ROOH$	$\rightarrow -\frac{15}{16}O_2 + \frac{7}{8}CO + \dot{O}H + H\dot{O}O$	$8.40\ 10^{14}$	0.00	180.03
12	$\dot{R} + O_2$	$\rightarrow -\frac{7}{16}O_2 + \frac{7}{8}CO + H\dot{O}O$	$2.00\ 10^{6}$	0.00	25.10
13	$RH + H\dot{O}O$	$\rightarrow \dot{R} + HOOH$	$4.11\ 10^{5}$	0.26	70.77
14	$RH + \dot{O}$	$\rightarrow \dot{R} + \dot{O}H$	$2.15\ 10^{6}$	0.31	21.13
15	$O_2 + \dot{H}$	$\rightarrow \dot{O}H + \dot{O}$	$2.00\ 10^{8}$	0.00	70.30

Table 2: Rate coefficients ... (continued)

			A	β	E_a
16	$\dot{O}H + \dot{O}$	$\rightarrow O_2 + \dot{H}$	$1.46\ 10^{7}$	0.00	2.08
17	$H_2 + \dot{O}$	$\rightarrow \dot{O}H + \dot{H}$	$5.06\ 10^{-2}$	2.67	26.30
18	$\dot{O}H + \dot{H}$	$\rightarrow H_2 + \dot{O}$	$2.24\ 10^{-2}$	2.67	18.40
19	$H_2 + \dot{O}H$	$\rightarrow H_2O + \dot{H}$	$1.00\ 10^{2}$	1.60	13.80
20	$H_2O + \dot{H}$	$\rightarrow H_2 + \dot{O}H$	$4.45\ 10^{2}$	1.60	77.13
21	$\dot{O}H + \dot{O}H$	$\rightarrow H_2 + \dot{O}$	$1.50\ 10^{3}$	1.14	0.42
22	$H_2 + \dot{O}$	$\rightarrow \dot{O}H + \dot{O}H$	$1.51\ 10^{4}$	1.14	71.64
23	$\dot{H} + \dot{H} + M$	$\rightarrow H_2 + M$	$1.80\ 10^{6}$	-1.00	0.00
24	$H_2 + M$	$\rightarrow \dot{H} + \dot{H} + M$	$6.99\ 10^{12}$	-1.00	436.08
25	$\dot{O}H + \dot{H} + M$	$\rightarrow H_2O + M$	$2.20\ 10^{10}$	-2.00	0.00
26	$H_2O + M$	$\rightarrow \dot{O}H + \dot{H} + M$	$3.80\ 10^{17}$	-2.00	499.41
27	$\dot{O} + \dot{O} + M$	$\rightarrow O_2 + M$	$2.90\ 10^{5}$	-1.00	0.00
28	$O_2 + M$	$\rightarrow \dot{O} + \dot{O} + M$	$6.81\ 10^{12}$	-1.00	496.41
29	$O_2 + \dot{H} + M$	$\rightarrow H\dot{O}O + M$	$2.30\ 10^{6}$	-0.80	0.00
30	$H\dot{O}O + M$	$\rightarrow O_2 + \dot{H} + M$	$3.26\ 10^{12}$	-0.80	195.88
31	$H\dot{O}O + \dot{H}$	$\rightarrow \dot{O}H + \dot{O}H$	$1.50\ 10^{8}$	0.00	4.20
32	$\dot{O}H + \dot{O}H$	$\rightarrow H\dot{O}O + \dot{H}$	$1.33\ 10^{7}$	0.00	168.30
33	$H\dot{O}O + \dot{H}$	$\rightarrow O_2 + H_2$	$2.50\ 10^{7}$	0.00	2.90
34	$O_2 + H_2$	$\rightarrow H\dot{O}O + \dot{H}$	$6.84\ 10^{7}$	0.00	243.10
35	$H\dot{O}O + \dot{H}$	$\rightarrow H_2O + \dot{O}$	$3.00\ 10^{7}$	0.00	7.20
36	$H_2O + \dot{O}$	$\rightarrow H\dot{O}O + \dot{H}$	$2.67\ 10^{7}$	0.00	242.52
37	$H\dot{O}O + \dot{O}$	$\rightarrow O_2 + \dot{O}H$	$1.80\ 10^{7}$	0.00	-1.70
38	$O_2 + \dot{O}H$	$\rightarrow H\dot{O}O + \dot{O}$	$2.18\ 10^{7}$	0.00	230.61
39	$\dot{O}H + H\dot{O}O$	$\rightarrow O_2 + H_2O$	$6.00\ 10^{7}$	0.00	0.00
40	$O_2 + H_2O$	$\rightarrow \dot{O}H + H\dot{O}O$	$7.31\ 10^{8}$	0.00	303.53
41	$H\dot{O}O + H\dot{O}O$	$\rightarrow O_2+$	$2.50\ 10^{5}$	0.00	-5.20
42	$\dot{O}H + \dot{O}H + M$	$\rightarrow HOOH + M$	$3.25\ 10^{10}$	-2.00	0.00
43	$HOOH + M$	$\rightarrow \dot{O}H + \dot{O}H + M$	$9.87\ 10^{17}$	-2.00	206.80
44	$\dot{H} + HOOH$	$\rightarrow H_2 + H\dot{O}O$	$1.70\ 10^{6}$	0.00	15.70
45	$H_2 + H\dot{O}O$	$\rightarrow \dot{H} + HOOH$	$1.15\ 10^{6}$	0.00	80.88
46	$\dot{H} + HOOH$	$\rightarrow H_2O + \dot{O}H$	$1.00\ 10^{7}$	0.00	15.00
47	$H_2O + \dot{O}H$	$\rightarrow \dot{H} + HOOH$	$2.67\ 10^{6}$	0.00	307.51
48	$\dot{O} + HOOH$	$\rightarrow \dot{O}H + H\dot{O}O$	$2.80\ 10^{7}$	0.00	26.80
49	$\dot{O}H + H\dot{O}O$	$\rightarrow \dot{O} + HOOH$	$8.40\ 10^{6}$	0.00	84.09
50	$\dot{O}H + HOOH$	$\rightarrow H_2O + H\dot{O}O$	$5.40\ 10^{6}$	0.00	4.20
51	$H_2O + H\dot{O}O$	$\rightarrow \dot{O}H + HOOH$	$1.63\ 10^{7}$	0.00	132.71
52	$CO + \dot{O}H$	$\rightarrow CO_2 + \dot{H}$	4.40	1.50	-3.10
53	$CO_2 + \dot{H}$	$\rightarrow CO + \dot{O}H$	$6.12\ 10^{2}$	1.50	94.10
54	$CO + H\dot{O}O$	$\rightarrow CO_2 + \dot{O}H$	$2.70\ 10^{7}$	0.00	98.70
55	$CO_2 + \dot{O}H$	$\rightarrow CO + H\dot{O}O$	$3.32\ 10^{8}$	0.00	359.90
56	$CO + \dot{O} + M$	$\rightarrow CO_2 + M$	$1.00\ 10^{1}$	0.00	-9.70
57	$CO_2 + M$	$\rightarrow CO + \dot{O} + M$	$2.39\ 10^{9}$	0.00	515.60
58	$O_2 + CO$	$\rightarrow CO_2 + \dot{O}$	$2.50\ 10^{6}$	0.00	200.00
59	$CO_2 + \dot{O}$	$\rightarrow O_2 + CO$	$2.54\ 10^{7}$	0.00	228.90